Swiss J Geosci (2017) 110:67–84
DOI 10.1007/s00015-016-0243-2

Tectonic structure of the "Main Fault" in the Opalinus Clay, Mont Terri rock laboratory (Switzerland)

David Jaeggi[1] · Ben Laurich[2] · Christophe Nussbaum[1] · Kristof Schuster[3] · Peter Connolly[4]

Received: 11 April 2016 / Accepted: 9 December 2016 / Published online: 17 January 2017

Abstract Over the last 18 years we have extensively studied an intra-Opalinus Clay fault zone that crops out within the Mont Terri rock laboratory in NW-Switzerland. We performed micro- and macrostructural characterization on four outcrops of this so-called "Main Fault", which crosscuts the entire Mont Terri rock laboratory. Combining detailed structural mapping, analysis down to the nanometer-scale, and geophysical investigations leads to a better understanding of fault zones within clay-dominated lithologies. The multi-scale, multi-technique approach that we applied in this study on four individual outcrops is critical for describing such a complex system. In these four outcrops, we differentiate five macroscopic structural elements of the Main Fault and have studied their occurrence and spatial distribution. In general, scaly clay, including S–C bands (S = "schistosité" = cleavage, C = "cisaillement" = shear parallel to shear zone boundaries) and microfolds, occurs in isolated, sharply bound lenses and in larger zones at the top and bottom of the Main Fault. A cm-thin, continuous layer of gouge runs along the upper boundary of the fault zone. The non-scaly part shows rather low strain and consists of rhombohedral blocks of undeformed rock (horses), bound by slickensides. The µm-thin shear zones are considered to be elementary building blocks for the structural elements of the Main Fault. Direct comparison of the four studied outcrops to each other highlights the significant lateral variability of the Main Fault. In addition to a reduction in thickness from west to east, size and distribution of structural elements are highly variable. Correlation of these structural elements between closely spaced outcrops is not possible. Fortunately, the upper and lower boundary of the Main Fault, as well as thicker sheets of scaly clay, can be recognized using seismic attributes and thus yield indirect information about size and internal structure of fault zones in clay.

Keywords Mont Terri rock laboratory · Structural elements · Scaly clay · Microstructure · Clay gouge · p-wave velocity

Editorial handling: P. Bossart and A. G. Milnes.

This is paper #3 of the Monte Terri Special Issue of the Swiss Journal of Geosciences (see Bossart et al. 2017, Table 3 and Fig. 7)

✉ David Jaeggi
david.jaeggi@swisstopo.ch

[1] Federal Office of Topography swisstopo, Seftigenstrasse 264, 3084 Wabern, Switzerland

[2] Institute for Structural Geology, Tectonics and Geomechanics, RWTH-Aachen, Aachen, Germany

[3] Federal Institute for Geosciences and Natural Resources BGR, Stilleweg 2, 30655 Hannover, Germany

[4] CHEVRON, Rock Mechanics Team, Chevron ETC, 1500 Louisiana Street, Houston, TX 77002, USA

1 Introduction

The Mont Terri Project is an international research organisation, which aims to investigate and analyse the hydrogeological, geochemical and rock mechanical properties of the argillaceous Opalinus Clay Formation. This formation has been selected in Switzerland as the preferred host rock for the disposal of high-level radioactive waste. Furthermore its properties, described in detail in Bossart and Thury (2008) and Bossart et al. (2017), are ideal for experiments dealing with borehole integrity and CO_2 sequestration. Beside the inherent properties of the host rock, e.g. low permeability, high retention capacity for

radio-nuclides, and self-sealing of artificially induced fractures, faults and fault zones are important elements that might influence the evolution of a repository. Examples of large-scale fault settings in shales exist from studies of décollement zones of clay-rich accretionary prisms and tectonic mélanges: in the Barbados e.g. Housen et al. (1996), Labaume et al. (1997), and more recently in the Tohoku subduction zone e.g. Chester et al. (2013) and in the Alps e.g. Dielforder et al. (2015). Recent work focusing on the small-scale geometry and petrophysical properties of a fault zone in shale is available from the Tournemire site, e.g. Dick et al. (2016). These authors show that strain inferred from anisotropy of magnetic susceptibility indicate heterogeneous structural fabrics within the fault core. In the Opalinus Clay, faults and fault zones were investigated hydraulically by Marschall et al. (2004; 2005) who showed that permeability of faulted Opalinus Clay does not differ significantly from the undisturbed rock.

Faults and fault zones have a significant influence on the stability of galleries and the geometry of the excavation damaged zone (EDZ) (Yong et al. 2010; Thoeny 2014). The EDZ develops during the excavation of new galleries and is a zone where stress redistribution and subsequent rock convergence result in a network of unloading fractures. Geophysical investigations, e.g. ultrasonic measurements, have aided in the detection of high fault densities and fault zones (Schuster 2012). Further investigations have concentrated on macroscopic structure and the evolution of the faults and fault zones in the local and regional tectonic setting (Nussbaum et al. 2001, 2011). Recently, within the framework of the PS (Petrofabric and Strain) experiment, work focused on pore structure (Houben et al. 2013) and assessment of microscale to nanoscale characterisation of faults and fault zones. Laurich et al. (2014) found that the elementary building blocks of the Main Fault are thin localized shear zones of <4 μm width. They also found that with progressive deformation, number and density of slickenside shear surfaces increases, generating tectonically derived scaly clay and more homogeneous gouge. In all deformed elements of the Main Fault porosity is reduced compared to undeformed Opalinus Clay, resulting in local permeability barriers for pore water pressure dissipation. During the formation/activity of the Main Fault, such permeability barriers could have led to differential pore water pressures, which in turn could have controlled the evolution and distribution of structural elements.

The present study integrates the microstructural knowledge from the comprehensive work of Laurich (2015) with the macroscopic structure observed at the outcrop-scale (Nussbaum et al. 2001, 2011) in order to generate a synthetic geometrical model of a fault zone in Opalinus Clay. The final part of this study attempts to correlate the observed structural elements with ultrasonic and structural data from a borehole crossing the Main Fault close to one of the studied outcrops. Characterising the lateral variation and distribution of structural elements within a fault zone and recognising their signature on geophysical logs is critical for understanding overall rock-mass behaviour and repository evolution.

Fig. 1 **a** Location of Mont Terri rock laboratory, **b** tectonic overview ▶ of the Mont Terri area, **c** location of the Mont Terri rock laboratory on the geological cross section

2 Geological setting

The Mont Terri rock laboratory is located in the Toarcian–Aalenian Opalinus Clay in the southern limb of the Mont Terri anticline about 300 m below the surface. The Opalinus Clay can be divided into a shaly facies, a sandy facies, and a carbonate-rich sandy facies (Blaesi et al. 1996; Bossart and Thury 2008; Hostettler et al. 2017) with varying contents of clay minerals, quartz, and carbonate. Bedding dips SSE between 50° in the southern part to 30° in the northern part. The anticline, which formed in the Late Miocene and Pliocene, is regarded as a fault-bend fold developed above a frontal ramp and features an overturned forelimb. This forelimb is affected by a complex pattern of thrust faults, extensional faults, and strike-slip faults (Nussbaum et al. 2011). The main detachment is located within the Middle Triassic evaporites; Zeglingen Formation (Fig. 1). Towards the WNW, the fold axis is approximately perpendicular to the SSE > NNW principal horizontal stress direction, present during the Middle Miocene Jura thrusting phase. Towards the WSW, the anticline bifurcates into two anticlines, of which the northern branch is intersected by a sinistral strike-slip fault. The two branches form a lateral or oblique ramp towards the west. Three major fault systems are present in the Mont Terri rock laboratory: SSE-dipping faults that run parallel or sub-parallel to the bedding, flat to SW-dipping faults, and steep N-NE-striking faults (Fig. 2).

The most prominent tectonic feature of the rock laboratory is the so-called Main Fault, a thrust fault located in the shaly facies of the Opalinus Clay with shear movement towards NNW. The Main Fault crosses the two galleries Ga08 and Ga98 at almost right angles (Fig. 2). These two galleries are trending SSE–NNW and are oriented approximately perpendicular to fold axis and strike of bedding. According to Nussbaum et al. (2011), the Main Fault zone consists of several architectonic elements: fault gouge, S–C bands (S = "schistosité" = cleavage, C = "cisaillement" = shear parallel to shear zone boundaries), meso-scale folds, microfolds, numerous fault planes, and apparently undeformed segments. The thickness of the fault zone varies laterally between 1 and 4.5 m.

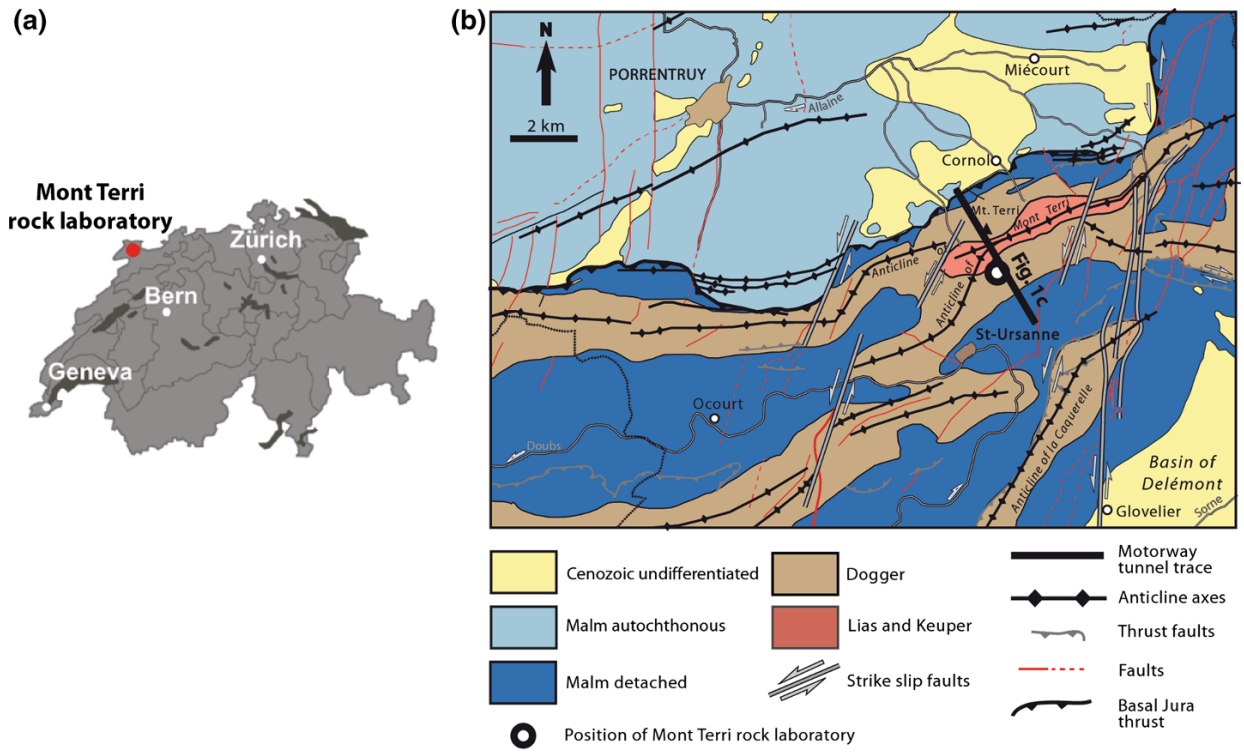
(a)
Mont Terri
rock laboratory
Zürich
Bern
Geneva
(b)
N
2 km
PORRENTRUY
Allaine
Miécourt
Cornol
Mt. Terri
Mont Terri
Anticline
Anticline of
Fig. 1c
St-Ursanne
Ocourt
Doubs
Basin of
Delémont
Anticline of la Caquerelle
Glovelier
Sorne
Cenozoic undifferentiated
Malm autochthonous
Malm detached
Position of Mont Terri rock laboratory
Dogger
Lias and Keuper
Strike slip faults
Motorway
tunnel trace
Anticline axes
Thrust faults
Faults
Basal Jura
thrust

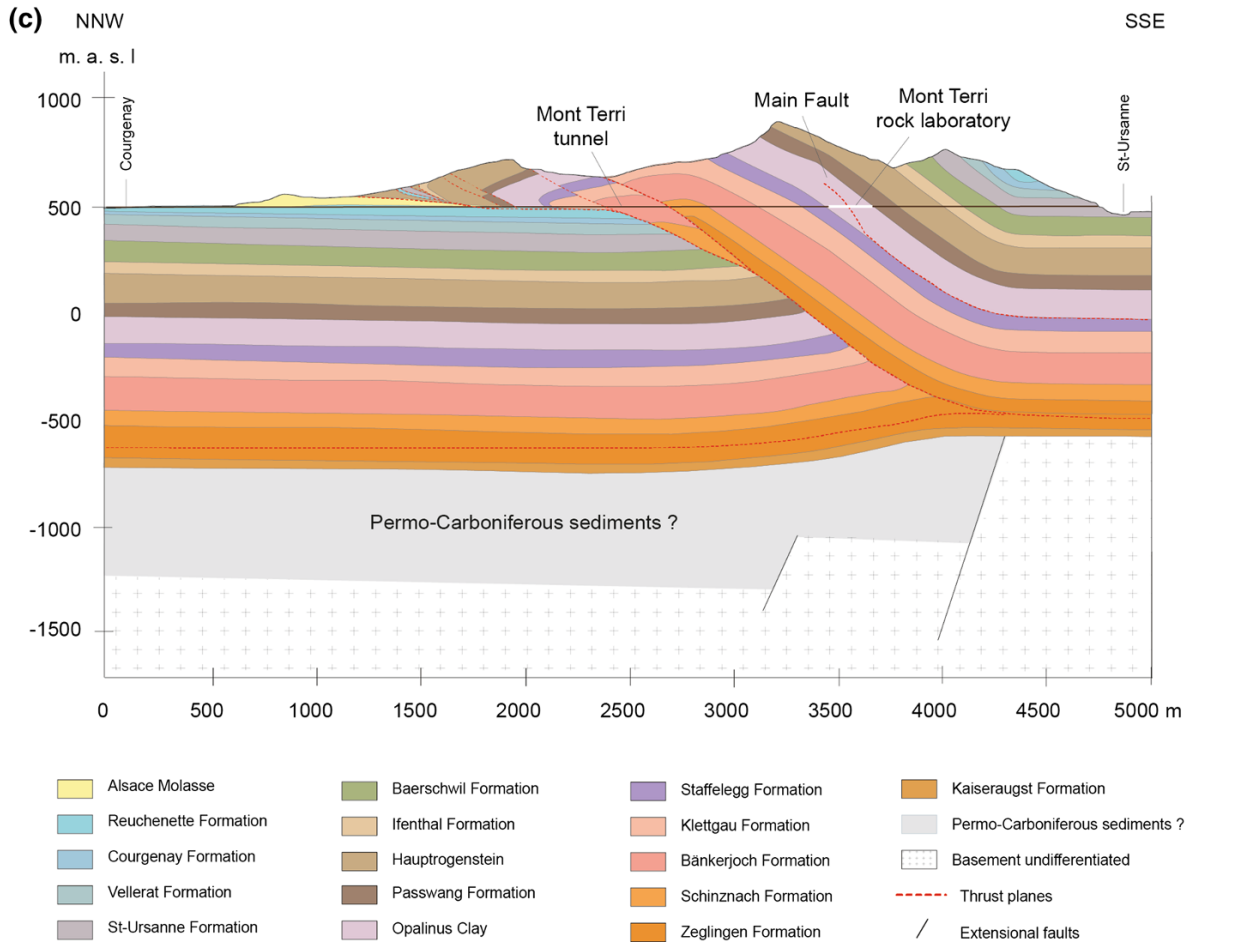
(c)
NNW
SSE
m. a. s. l
1000
500
0
-500
-1000
-1500
Courgenay
Mont Terri
tunnel
Main Fault
Mont Terri
rock laboratory
St-Ursanne
Permo-Carboniferous sediments ?
0
500
1000
1500
2000
2500
3000
3500
4000
4500
5000 m
Alsace Molasse
Reuchenette Formation
Courgenay Formation
Vellerat Formation
St-Ursanne Formation
Baerschwil Formation
Ifenthal Formation
Hauptrogenstein
Passwang Formation
Opalinus Clay
Staffelegg Formation
Klettgau Formation
Bänkerjoch Formation
Schinznach Formation
Zeglingen Formation
Kaiseraugst Formation
Permo-Carboniferous sediments ?
Basement undifferentiated
Thrust planes
Extensional faults

Upper and lower fault boundaries dip 40°–45° towards SSE in Ga08 and 50°–55° towards SSE in Ga98. In the footwall of the fault, mainly subhorizontal fault planes are present, whereas SW-dipping faults are found in the hanging wall. For more detailed information about the geological context the reader is referred to Nussbaum et al. (2011) and Hostettler et al. (2017).

3 Materials and methods

3.1 Structural mapping of outcrops

We investigated the outcrops by structural small-scale mapping. Mapping was aided by applying a grid overlay to each exposure. The size of the grid elements ranged from 1.0 to 0.2 m depending on the exposure's surface area (size). Before mapping, the rock surface was carefully cleaned of dust and shotcrete patches. We photographed the entire outcrop surface and directly marked structural features on the photos. For easier comparison of size, variability and distribution of structural elements, the outcrop images are all presented at the same scale and are viewed from SW to NE. Thus, outcrops on the eastern side of the gallery are viewed from the gallery ("view towards rock") and outcrops on the opposite, western, side of the gallery are viewed from within the rock ("view towards gallery"). Their maps are, by necessity, horizontally mirrored. The outcrops on opposite sides of a gallery are 4 m apart and the two galleries Ga98 and Ga08 are 40 m apart.

3.2 Microscopic analysis

We extracted resin-stabilized drillcores and hand specimens from the different outcrops of the Main Fault. Exact sampling locations and detailed descriptions of the applied methods are given in Laurich et al. (2014) and Laurich (2015). Samples were investigated by optical and scanning electron microscopy (SEM) in surface (i.e. looking on the fault plane) and section views. Samples were split along slickensides, cut by hand, polished and water-immersed for 2 s. Water immersion results in a fine decoration of the

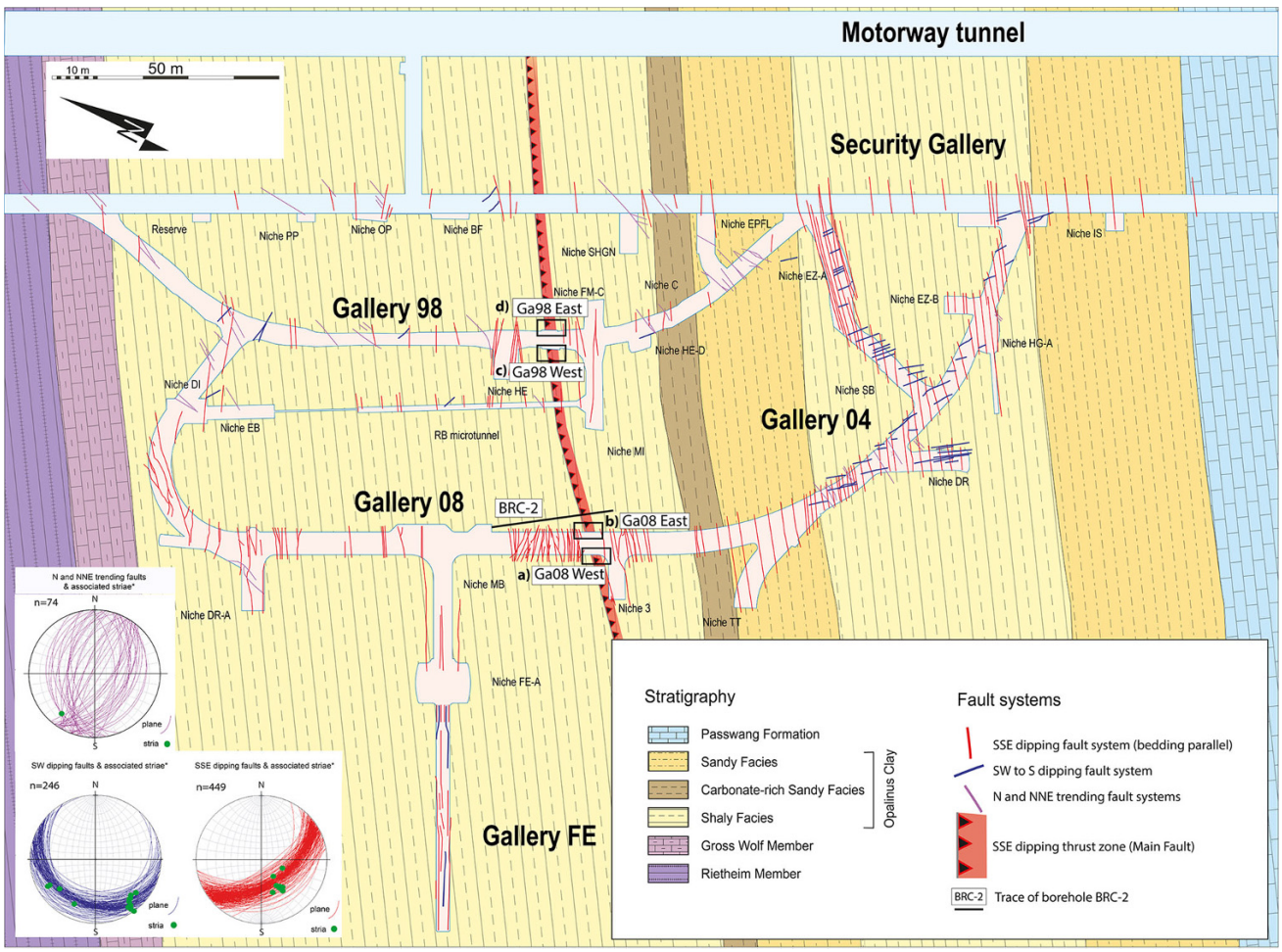

Fig. 2 *Horizontal view* of the Mont Terri rock laboratory with locations of the four investigated outcrops *a–d* and the trace of borehole BRC-2

foliation by the swelling clay matrix and thus helps to highlight fine structures. Ultra-thin sections followed by hand-polishing were produced. Finally, broad-ion beam polishing (BIB) and cutting transmission electron microscopy (TEM) lamellae by focused ion beam (FIB) were the methods used to investigate the microstructure.

3.3 Seismic characterization of fault zones by means of ultrasonic measurements

Continuous single-hole ultrasonic interval velocity measurements (IVM) were performed in borehole BRC-2 immediately after drilling. A BGR mini-sonic probe was utilized as shown in Fig. 3a. The centre frequency of the emitted signal was 50 kHz. The probe consists of four linearly distributed piezoelectric transducers. One transducer is used as the seismic source with the remaining three used as receivers at distances of 10, 20 and 30 cm from the source. Coupling of the transducers at the borehole wall was done using pneumatic cylinders. Measurements were conducted from top to bottom of the borehole and located at intervals of 10 cm. The borehole was oriented horizontally with an azimuth of 144°, consequently cutting the bedding at an angle of 40°. Inside the borehole the tool was orientated at 3 o’clock, thus measuring horizontally into the borehole wall towards Ga08 (Fig. 2).

Seismic velocities and amplitudes derived from initial p- and s-wave arrivals were calculated according to traveltimes and distances, assuming straight ray propagation (Fig. 3b, c). As an unavoidable result of the drilling, we had to take into account a borehole disturbed zone (BdZ) with radial velocity gradients (Schuster et al. 2017). Therefore, these velocities are treated as apparent velocities. Differences between these apparent velocities allow calculation of a BdZ corrected Vp, which enables investigation of the region beyond the BdZ. The BdZ-corrected Vp represents the Vp of the intact rock. The extent of the BdZ can reach several cm (Schuster 2012). Additionally, we calculated elastodynamic parameters like dynamic Young’s modulus via receiver R3 (30 cm distance) data, which are generally very close to the BdZ-corrected parameters.

In the shaly facies of the anisotropic Opalinus Clay, Vp perpendicular to bedding is 2600 m/s and parallel to bedding 3400 m/s. With borehole orientation of BRC-2 perpendicular to the strike of the bedding and the tool measuring horizontally along the 40° dipping beds, a Vp of 2700 m/s is a good average value for undisturbed Opalinus Clay (Schuster et al. 2017). Any deviation from average values, is an indication of a change in elastic rock properties, such as micro- and macroscopic disturbances or damage, lithological changes and tectonised structures. Furthermore in strongly tectonised sections, such as scaly clay, the orientation of the foliation can change dramatically, which could in turn affect Vp.

4 Characteristics of the fault zones in the Mont Terri rock laboratory

4.1 Structural elements observed on the Main Fault and microscopic structure

Deformation in compacted clay sediments is usually localized in µm-thin shear zones and corresponding slickensides. Haines et al. (2013) describe the evolution of a thin shear zone with increasing shear. At the end of the linear part of the stress–strain curve, en echelon Riedel-

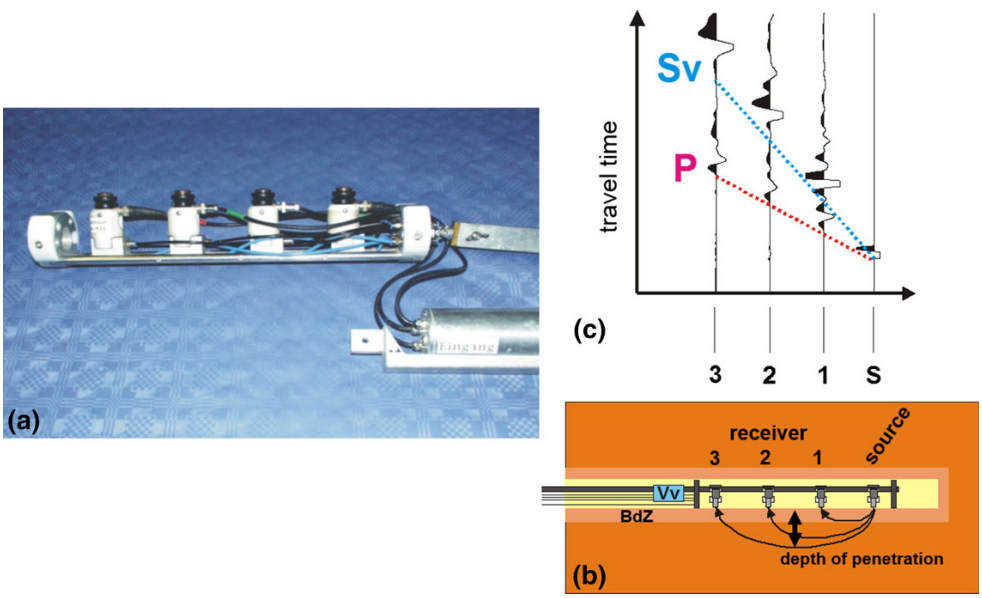

Fig. 3 Principle of interval-velocity measurements (IVM). **a** BGR 4KUBS ultrasonic borehole probe, **b** seismic-ray propagation (schematic), **c** single shot section with P-wave arrivals (*P*) and vertically polarised shear-wave arrivals (*Sv*)

shears (R-shears) and shear-sense parallel Y-shears develop. These initially propagate towards the boundaries of the deformed layer and rotate further during post-peak stress or strain softening. During stable sliding at residual shear strength, where the material exhibits a perfectly plastic behaviour, a pervasive network of R-shears and Y-shears develops (Passchier and Trouw 1996). During further straining, the R-shears become undulatory and internal deformation occurs within the shear bounded packages. The rheology of shales appears to be scale dependent and thus phenomenological terms like "brittle" and "ductile" are a function of scale (Ismat 2013) and strain rate. Heterogeneities, such as larger pores or stiffer particles within the clay matrix act to localize early deformation. In the Opalinus Clay, fractures initiate mainly at grain boundaries and edges of coarse shell fragments (Klinkenberg et al. 2009). The mechanical behaviour of Opalinus Clay is strongly dependent on the content and distribution of bioclastic and detritic material. Furthermore, it is different for each lithofacies type. In the shaly facies, heterogeneities of bioclastic material act as nuclei for fracture growth and thus reduce the strength of the rock. In contrast, higher carbonate content in the sandy facies leads to increased rock-mechanical strength (Gschwind 2013). Laurich et al. (2014) found indicators for at least five different deformation mechanisms: (1) dissolution and precipitation creep, (2) rigid body rotation and particle sliding, (3) cataclasis, (4) intra-crystalline plasticity, and (5) new formation of clay minerals. In the next section, we describe the main structural elements observed in Opalinus Clay: isolated slickensides, gouges and scaly clay comprising microfolds, and S–C bands.

4.1.1 Slickensides (and thin shear zones)

Shiny, striated slickensided surfaces (sensu Blenkinsop 2000) occur especially in fault zones throughout the Opalinus Clay at Mont Terri (Fig. 2) and are present as smooth planar surfaces (Fig. 4a, b). Magnifications of up to 100 kx SEM show sub-µm to nm-sized clay particles aligned parallel to slickensides in section view (Fig. 4c, d). According to Clauer et al. (2017), chemical and isotopic analyses suggest that some of these clay particles can be interpreted as newly formed illite. The lateral extent of the slickensides ranges between µm and 1 m. Laurich (2015) presented eight slickenside kinematic indicators, such as different kinds of grooves, steps, and striae, all of which are consistent with a compressive regime. With increasing spatial frequency of slickensides, they become more curved and undulating, forming microfolds, S–C shear bands, and crenulation cleavage (sensu Passchier and Trouw 1996) in scaly clay aggregates. In section, slickensides are associated with µm-wide shear zones of parallel-aligned clay particles (Fig. 4c, d). There, the shear zone internal porosity is drastically reduced when compared to the undeformed host rock.

Slickensides exhibit polished, dark, and shiny areas as well as more bright, ragged, and dull parts. These spatial variations are caused by variation in calcite content, which is low in restraining and high in releasing parts of the slickensided surfaces (Laurich et al. 2014; Laurich 2015). The latter manifest as risers of slickenside steps (Doblas et al. 1997), at which patches of calcite form (Fig. 4a). Occasionally slickenfibers and concentric growth patterns can be seen, indicating syntectonic calcite growth. Furthermore, aligned clay particles usually cover the calcite patches, suggesting movement along µm-shear zones made of clay, while the calcite forms in a crack-seal manner (Koehn and Passchier 2000). Despite the patches, calcite and, more rarely celestite veins are often associated with slickensides. Conversely, wide-aperture veins within the Main Fault are rare and crosscutting relationships are not observed. In addition to calcite precipitations, agglomerations of pyrite can be found along the shear zones. According to Laurich (2015), micron-wide shear zones (Fig. 4c, d) and nano particles on slickensides are common structures and shear zones probably initiated and evolved as en-echelon networks of shear fractures.

4.1.2 Fault gouge

Fault gouge is found in up to 2 cm-thick continuous bands along the upper boundary of the Main Fault. Furthermore, it occurs as less prominent thin discontinuous bands and lenses in other parts of the Main Fault, but always related to scaly clay (Fig. 4e, f). Fault gouge is known to accommodate high strain particularly in parts with high offset. In the Opalinus Clay, the dark colour of gouge compared to the host rock is conspicuous. Based on microscopic analysis Laurich et al. (2014) found that the darker colour originates from decreased calcite content, finer particle size, and reduced porosity (Fig. 4e). Polished and shiny slickensides are often present at the gouge-wall rock boundary. We also found slickensides within the gouge. If the gouge material is crushed, it disintegrates into a fine powder along a set of anastomosing and overlapping shear zones (Laurich et al. 2014). The gouge is clearly depleted in calcite compared to the host rock or the neighbouring scaly clay. This is in marked contrast to non-gouge slickensides, where calcite is present at risers. Inside the gouge a P-foliation pattern with high fabric intensity is present. Laurich et al. (2014) differentiated gouge with a high angle between P-foliation and shear-zone dip (type 1) from gouge with almost parallel angle between P-foliation and shear zone dip (type 2). Veins are rare inside the gouge but they also occur frequently along the gouge boundary.

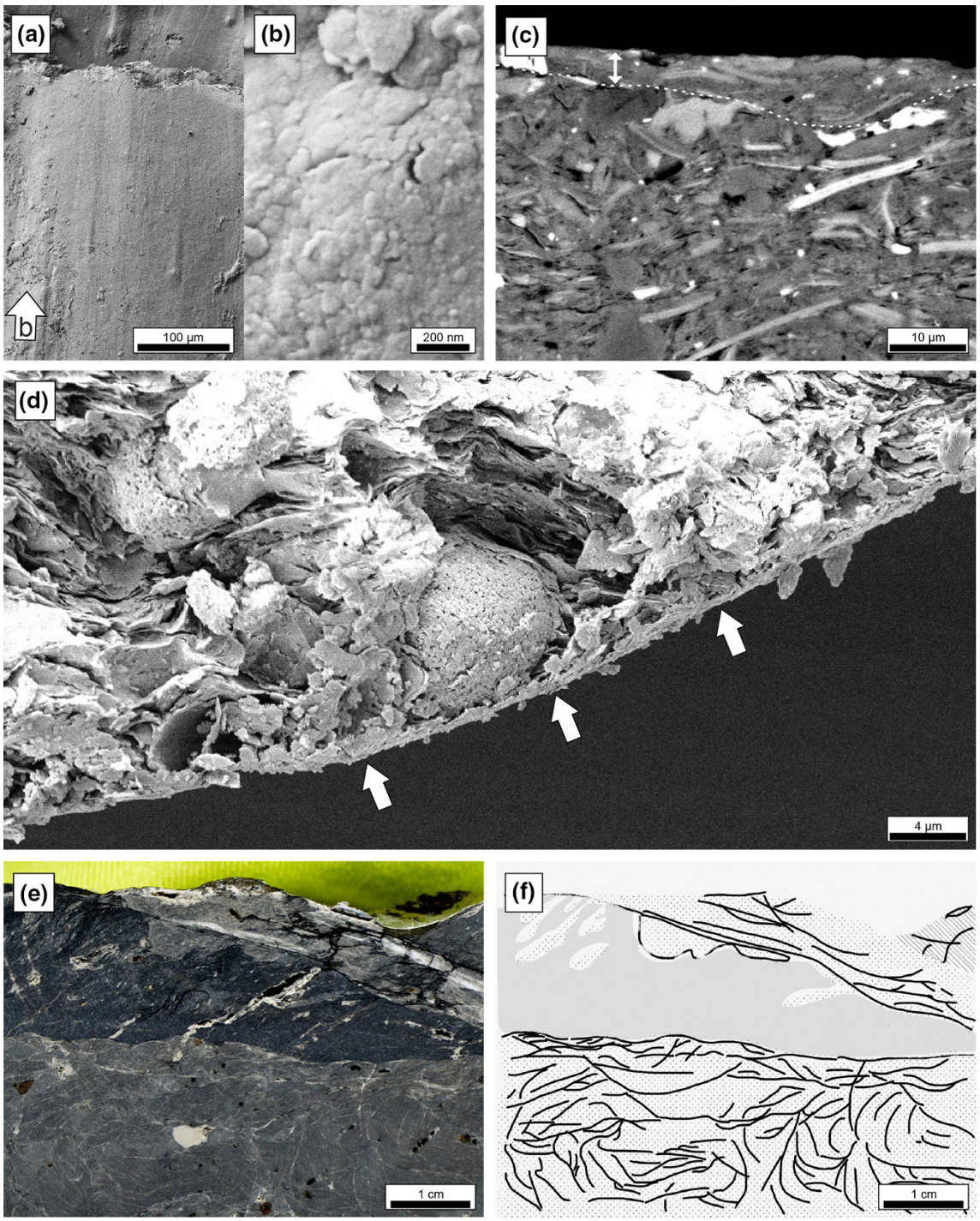

Fig. 4 **a** SEM micrograph of a polished surface with slickensides in *top view*. A slickenside riser perpendicular to shear direction can be seen in the *upper part* of the image with linear striae visible (*arrow* **b**) parallel to slip direction. **b** High-resolution SEM micrograph of **a** showing nm-wide, platy clay particles aligned parallel to the slickensided surface. **c** BIB–SEM micrograph of a µm-thin shear zone in side view (*above dashed line*). Note the shear zone-parallel alignment of clay minerals. Authigenic illite can be seen as thin curvy fibres *above the dashed line*. Location of micrograph is given in Fig. 5d. **d** SEM image showing side view of a slickenside with a nano-sized thin band of clay particles (indicated by *arrows*), possibly authigenic illite. **e** Photograph and **f** sketch of a gouge band from the upper boundary of the Main Fault. The darker gouge is sharply separated by µm-thin shear zones from bordering scaly clay. Note the brighter clasts of scaly clay within the gouge. *Dark lines* in **f** are traced shears

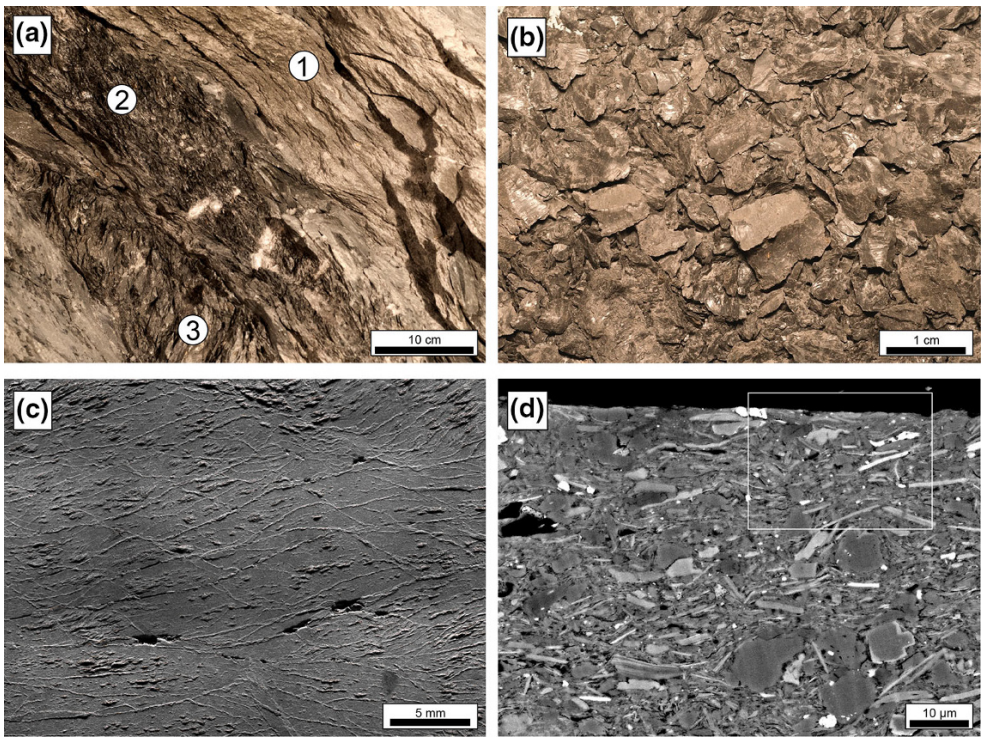

Fig. 5 **a** Photograph of outcrop in gallery 98, view direction towards ENE. *1* Mostly undeformed Opalinus Clay sectioned by solitary slickensides, *2* highly fissile scaly clay (=high degree of "scaliness"), *3* S–C band, width up to 10 cm. **b** Photograph of loose scaly clay microlithons with shiny polished surfaces. **c** Photograph of a water-immersed sample showing the anastomosing shear-zone network that encapsulates microlithons of various sizes. **d** BIB–SEM micrograph of the internal structure of a microlithon. The fabric resembles that of undeformed shaly Opalinus Clay. *White inset* is shown in Fig. 4c

Laurich et al. (2014) analyzed 8 gouge samples with XRD. All samples revealed a significant reduction in calcite content, while all other mineral phases remain comparable to the host rock.

Gouge microstructures revealed indicators for cataclastic evolution accompanied by calcite pressure solution, strong particle reorientation, and formation of internal thin shear zones, presumably at later stages of gouge formation (Laurich et al. 2014). The occurrence of frequently healed and occasionally strained calcite veins in the surrounding of gouge indicates that during the evolution of the gouge, the deformation mechanism changed from purely frictional cataclasis to frictional-viscous pressure solution. The sharp boundaries of gouge are explained by intensive straining of the µm-thin shear zones that border the gouge, leading to abrasion and calcite dissolution of a thin layer of wall rock. We hypothesise that the decreased grain size within the gouge amplifies pressure-solution compared to the host rock (Gratier et al. 2014) and that the calcite re-precipitated as veins in the gouge surroundings. However, recent isotope analysis indicates that gouge-associated fluids might also have played a role in calcite dissolution (Clauer et al. 2017).

4.1.3 Scaly clay (microfolds, S–C bands)

Highly strained Opalinus Clay aggregates from the Main Fault can be broken by hand into progressively smaller lensoid flakes that are bound by shiny polished slickensided surfaces (Fig. 5b). This fabric is called scaly clay (sensu Vannucchi et al. 2003). According to Laurich (2015), it consists of a tangled, interconnected web of slickensides that bound largely unaltered microlithons (Figs. 4c, 5d). Thus, the scaly clay formed by finely distributed shear, leaving a ductile impression of microfolds and S–C bands at the macroscopic scale (Fig. 5a). The retrieval of scaly clay samples that maintain their integrity is difficult and rarely achieved. Within the rock mass, scaly clay is subjected to in situ stress, where at rock lab level sigma 1 is controlled by the overburden. Once samples of scaly clay are extracted from the rock mass, stress relief and desiccation lead to fast decomposition of the material. Subjected to the in situ stress, scaly clay, and fault zones in general exhibit a hydraulic permeability, which does not differ significantly from the host rock (Marschall et al. 2004).

Zones with scaly clay fabric range from 0.01 to 1 m thickness. Scaly clay aggregates are sharply separated from

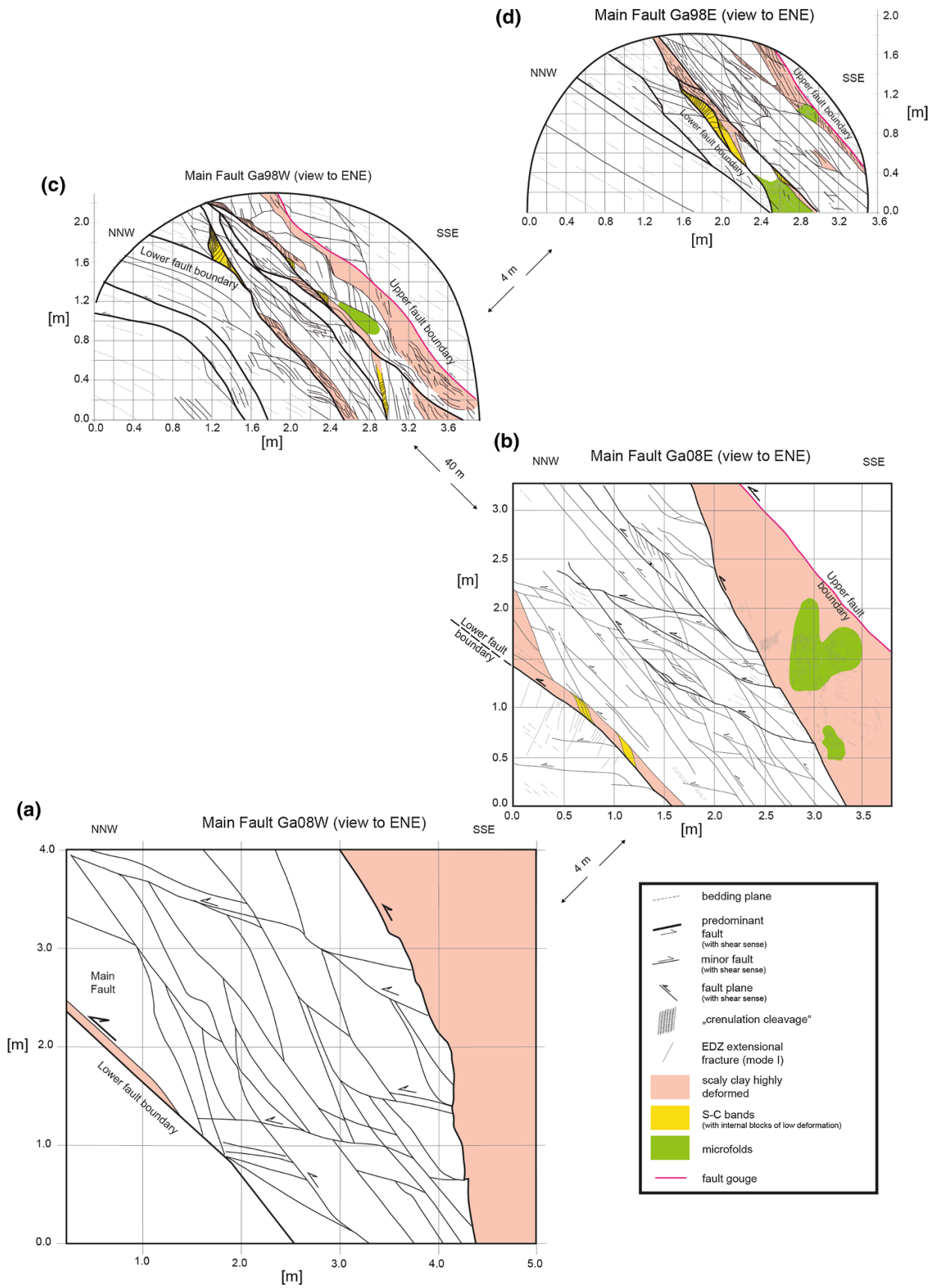
(d)
Main Fault Ga98E (view to ENE)
NNW
SSE
Upper fault boundary
Lower fault boundary
[m]
4 m
(c)
Main Fault Ga98W (view to ENE)
NNW
SSE
Lower fault boundary
Upper fault boundary
[m]
40 m
(b)
Main Fault Ga08E (view to ENE)
NNW
SSE
Upper fault boundary
Lower fault boundary
[m]
4 m
(a)
Main Fault Ga08W (view to ENE)
NNW
SSE
Main Fault
Lower fault boundary
[m]
bedding plane
predominant fault (with shear sense)
minor fault (with shear sense)
fault plane (with shear sense)
„crenulation cleavage“
EDZ extensional fracture (mode I)
scaly clay highly deformed
S-C bands (with internal blocks of low deformation)
microfolds
fault gouge

◀**Fig. 6** Comparison of macrostructures observed at four different outcrops of the Main Fault. Views are drawn at the same scale and oriented the same way for comparison with fault dip from *upper left towards lower right*. **a** Main Fault Ga08W (view towards tunnel), note that upper fault boundary is just *above the right corner* behind shotcrete, **b** Main Fault Ga08E (view towards rock), **c** Main Fault Ga98W (view towards tunnel), **d** Main Fault Ga98E (view towards rock)

the non-scaly fault parts by μm-thin shears. The formation of scaly clay is interpreted as a product of continuous deformation within local relays of linking shear zones (Laurich 2015). Three macroscopically different appearances of scaly clay can be observed: (1) anastomosing fabric with branching shears mostly subparallel to the borders of the fault zone with internal rotation of bedding foliation (Fig. 5c), (2) S–C fabrics, where particle reorientation between two opposite single shears led to prominent sigmoidal structures (Fig. 5a), and (3) microfolds (Fig. 6b). Many of these S–C fabrics show internal rigid blocks with larger undeformed domains. Calcite veins are commonly present in scaly clay, occurring as intact, fractured and strained morphologies suggesting early to syntectonic vein precipitation. By means of $^{87}Sr/^{86}Sr$ isotopic analysis, Clauer et al. (2017) could show that some of the veins observed in Opalinus Clay formed before the development of the Mont Terri anticline. Furthermore, from studies of accretionary prisms it is known that the combined effects of compaction and calcite cementation in overpressured and mechanically weak rocks, such as a shale, can lead to coseismic formation of veins (Dielforder et al. 2015).

As discussed above, due to shearing, the thin shear zones are less porous, thus reducing porosity. In a rock with very low permeability, where on the short-term pore water cannot escape, further shearing leads to localized increase of pore water pressure. This localized pressure build-up can hypothetically be a cause for the development of a dense shear zone network, while in other parts of the Main Fault there is no scaly clay, even where the mineralogy is very similar.

4.2 Macroscopic structural description of the Main Fault in Ga08

4.2.1 Outcrop in Ga08 Western side (view towards tunnel)

The windowed exposure on the western side of Ga08 does not contain the entire Main Fault since the upper fault boundary is now behind shotcrete. Fortunately, the upper fault boundary can be extrapolated from neighbouring windows quite precisely to the upper SSE-corner of the main window (Fig. 6a). The rectangular window is 5 m wide and 4 m high. The approximately 4.5 m thick Main Fault covers about 85% of the window, showing scaly clay and a zone of isolated slickensides. The upper part mainly consists of scaly clay with anastomosing structures, with no clear signs of microfolding or S–C bands. This zone exhibits a thickness of more than 2 m and covers about 53% of the area of the entire Main Fault (Table 1). The lower boundary, towards the zone of isolated slickensides, shows a reduction in dip from bottom to top of the window from 80° to 60°, respectively. The lower part (47%) of the Main Fault in this westernmost outcrop consists of a broadly spanned network of slickensides building rhombohedral and internally undeformed blocks of 0.1–1 m size. This zone exhibits a thickness varying from 2 m at the lower part to 3 m in the upper part of the outcrop. The lower fault boundary has an average dip of 46°. In the NW-part of the lower boundary a 10 cm-thick non-continuous band of scaly clay is present.

4.2.2 Outcrop in Ga08 Eastern side (view towards rock)

The outcrop in Ga08 Eastern side is located about 4 m eastwards. The window covers an area of 3.8 × 3.3 m and shows the entire Main Fault. Lower and upper fault boundaries dip with 40°–45° to the SSE. The beds in the hanging wall and the footwall dip less than the shear-zone boundary. The thickness of the Main Fault here is about 2.7 m, significantly less than on the western side of the gallery 4 m away. At the eastern exposure we differentiate

Table 1 Relative-area percentages of structural elements for the four different outcrops of the Main Fault in the Mont Terri rock laboratory

Outcrop	Fault zone width (m)	Scaly clay (incl. microfolds + S–C bands) (%)	Isolated slickensides (%)	Microfolds (%)	S–C bands (%)
Ga08 W	4.5	53	47	–	–
Ga08 E	2.7	42	58	5	1
Ga98 W	1.0	37	63	2	4
Ga98 E	0.9	20	80	4	3

The entire area of the Main Fault at individual outcrops is equal to 100%. Percentage of scaly clay area includes anastomosing scaly clay and the inherent zones of microfolding and S–C bands. For the outcrop in Ga08W, the non-visible part of the Main Fault was included in the total surface area for consistency

five structural elements (Fig. 6b). The upper fault boundary consists of a cm-thick gouge marking the sharp transition from undeformed host rock to highly deformed scaly clay. The fault gouge is continuous and the internal structure is macroscopically poorly visible. Further into the Main Fault, there is a 1–1.5 m-thick zone of scaly clay, which is separated from the lower part by a distinctive reverse fault. The internal structure of the scaly clay is mainly anastomosing, evidencing occasional regions of microfolds with folded axes. Microfolds compose approximately 5% of the entire Main Fault area in this exposure (Table 1). Crenulation cleavage is also present. The next lower 1.5–2 m of the Main Fault is characterised by 0.01–0.1 m-scale rhombohedral undeformed blocks bounded by single sinistral slickensides. At some locations the morphologies expressed resemble incipient S–C bands, with some P-shears. No scaly clay occurs in this section of the Fault. Below the intra-fault section adjacent to the footwall, the outcrop consists of a 10 cm-thick continuous band of scaly clay with a sharp transition to the undeformed footwall. Here, the scaly clay exhibits zones with sigmoidal shapes indicating S–C banding.

In summary, shear bands comprise less than 1% of the entire Main Fault surface. Scaly clay, including shear bands and microfolds, covers about 42% of the entire Main Fault surface and isolated slickensides building rhombohedral blocks cover about 58%.

4.3 Macroscopic structural description of the Main Fault in Ga98

4.3.1 Outcrop in Ga98 Western side (view towards tunnel)

This horseshoe-shaped outcrop has the most complicated internal structure of the Main Fault exposed in the Mont Terri rock laboratory. The outcrop is 3.9 m wide and 2.3 m high with the Main Fault zone approximately 1.0 m thick representing undulating upper and lower boundaries. The upper fault boundary dips at 45° whilst the lower one dips at 52°. The lower fault boundary appears to flatten out towards the NNW (Fig. 6c). Bedding in the footwall is less inclined (30°–35°) than in the hanging wall (42°–46°). The upper fault boundary is characterised by a cm-thick gouge that occurs on top of a continuous band of scaly clay. The thickness of this scaly-clay band varies between 5 and 20 cm. Internally, other than an anastomosing fabric, we detect no specific features. Below, there is a 60–70 cm-thick heterogeneous zone of undeformed, mostly rhombohedral, 0.01–0.1 m-scale blocks bound by slickensides. Two major internal faults sub-parallel to the fault zone boundaries and a third interconnecting fault are also present. Unlike the Ga08 exposure, scaly clay occurs within this central part and includes regions of microfolding and S–C bands. Scaly clay is mainly concentrated along the internal major faults emphasising the importance of these internal major faults. Towards the footwall, the Main Fault zone is bordered by discontinuous scaly clay. In the upper left corner, a well-developed S–C band occurs, where the lower fault boundary bifurcates into two faults, one with a 20° dip and the other exhibiting 60° dip. This geometry is interpreted to result from the indentation of an undeformed wedge, which led to increased strain at the triple point and consequently the development of the S–C band. S–C bands comprise up to ca. 4% of the Main Fault area, and microfolds approximately 2% (Table 1). Scaly clay, including shear bands and microfolds, represents an area of 37%. The rest of the Main Fault consists of rhombohedral blocks bound by slickensides.

4.3.2 Outcrop in Ga98 Eastern side (view towards rock)

The horseshoe-shaped easternmost outcrop is 3.5 m wide and about 1.8 m high, has lower and upper fault boundaries with 55°–60° dip to the SSE and a thickness of the Main Fault of approximately 0.9 m (Fig. 6d). At the upper fault boundary there is a distinct cm-thick continuous fault gouge. Then, a max. 20 cm-thick zone of scaly clay occurs, generally with an anastomosing internal fabric and occasional regions of microfolding. In the lower right part of the scaly clay, slickensides with P-shear orientations are present, whereas in the upper part Y-shears seem to dominate. Below, a 50–60 cm-thick zone of isolated slickensides forming rhombohedral undeformed blocks of 0.01–0.1 m-scale occurs. At one location (x/y = 2.5/1.2 m), scaly clay from the upper part of the Main Fault branches into the zone of isolated slickensides. The scaly clay here encompasses a large internally undeformed block, which acted again as an indenter. At some other locations (e.g. x/y = 3.1/0.5 m) strain seems high enough for the formation of incipient scaly clay. The bottom part of the Main Fault comprises 20 cm-thick scaly clay. This band is interrupted by undeformed blocks. The region close to the undeformed footwall exhibits well-developed microfolds and a 0.8 m-long S–C band. This shear band has an internal structure with undeformed blocks (microlithons) bounded by sigmoidal slickensides. S–C bands and microfolds occupy 3 and 4% of the entire Main Fault, respectively (Table 1). Scaly clay, including microfolds and S–C bands, represents about 20% of the entire area. Rhombohedral blocks bound by isolated slickensides comprise the largest area of the fault.

4.4 Seismic parameter responses of fault zones in Opalinus Clay

Interval velocity measurements (IVM) react very sensitively to the occurrence and generation of microcracks (Schuster et al. 2017). Furthermore in strongly tectonised

sections, such as scaly clay, orientation of foliation and thus orientation relative to the anisotropic material can change dramatically, which could also affect Vp. We therefore assume that many of the structural elements identified within the Main Fault (scaly clay, shear bands, microfolds) modify this geophysical signal since they are small-scale discontinuities.

4.4.1 Borehole BRC-2

We analysed seismic responses (Vp, amplitude) along the BRC-2 borehole placing emphasis on the section crossing the Main Fault (Fig. 2). Borehole BRC-2 was drilled in April 2008 at GM94.5 along Gallery 08. The 131 mm-diameter borehole trends almost horizontally towards 152° with a slight dip of 1°. The 29.2 m long borehole crosses bedding at an angle of ca. 40° and is located ca. 3.5–4.0 m behind the Ga08E outcrop of the Main Fault. The Main Fault is encountered between drilling depths 18.3 and 21.5 m and has a dynamic Young's Modulus of <5GPa and a fault frequency of 20 faults/m (Thoeny 2014). Intact Opalinus Clay in the direction of borehole BRC-2 typically has a Vp of 2700 m/s (Schuster et al. 2017). Vp along the BRC-2 borehole varies between 2500 and 2700 m/s corresponding in general to undisturbed rock with a maxima of 2800 m/s and minima of 1900 m/s. Thoeny (2014) and Baur (2014) correlated the minima to single faults or fault zones. The maxima could, however, at least partly be correlated to accumulations of carbonate sands, containing bioclastic material (mostly bivalve debris). Periodic decrease of Vp by several hundreds of m/s and over several m length could be related to an upwards decrease in carbonate particle size and abundance. It is known from other boreholes crossing the sandy or carbonate-rich sandy facies that Vp can reach values of 4500 m/s due to increased stiffness associated with mineralogy, different sedimentary fabric, and cementation (Schuster et al. 2017). In core material, detection of major fault zones is sometimes challenging and not always clear. However, direct correlation of the borehole to the large outcrop of the Main Fault in Ga08E, just 3.5–4.0 m apart, is a unique opportunity to study the seismic behaviour in fault zones in more detail.

4.4.2 Correlation of seismic parameters in response to structural elements

With the unique configuration of a borehole located close and sub-parallel to a well-described fault zone, more detailed analysis of fault structure and fault geometry is possible than from core description or optical borehole images alone. Figure 7 shows Vp and the common offset gather (COF) including travel times and colour coded amplitudes of borehole BRC-2 in comparison with the structural map of the outcrop in Ga08E. Borehole BRC-2 is located about 3.5–4.0 m behind the outcrop at a projected level of about 2.1 m in the gallery. On core material and optical borehole imager, the Main Fault was encountered between 18.3 and 21.5 m depth. Two zones of scaly clay could be detected. A thin zone at the basis extends from 18.3 to 18.5 m and a second thicker one at the top of the Main Fault from 19.5 to 21.5 m. In the middle part, undisturbed blocks bound by single slickensides are present. Before considering Vp values, we note that BdZ-corrected Vp accounts for the stronger attenuation of Vp due to the enhanced pore space in the near field of the borehole. The corrected or improved Vp signal simultaneously allows for a higher penetration depth per time increment. Treated accordingly, the Vp signal of undisturbed Opalinus Clay yields values between 2400 and 2700 m/s at an angle of 40° between borehole and bedding planes. Between 18.3 and 18.5 m, a sudden decrease towards 2200 m/s is present. By investigating core material we were able to identify this as scaly clay that builds the lower fault boundary of the Main Fault. Below from 18.5 to 19.5 m single slickensides could be detected on core material, which yield a Vp of 2400 m/s. Then between 19.5 and 21.5 m, Vp is again mostly low, reaching values below 2000 m/s. On core material this zone can be attributed to a thick zone of scaly clay, which comprises the upper part of the Main Fault. On the COF the strong attenuation of the amplitude within these two zones of scaly clay is clearly highlighted (Fig. 7). At outcrop Ga08E, we can differentiate six different domains: undeformed foot- and hanging wall rock, scaly clay, S–C bands, microfolds, rhombohedral blocks bound by slickensides, and fault gouge. Scaly clay in the top part of the Main Fault of this outcrop is more than a metre thick and thus a prominent structural element. Furthermore, scaly clay of the lower fault boundary can also be identified clearly on IVM data. Microfolds, S–C bands, and gouges are too small and too patchy for reliable correlation to seismic responses.

Comparing borehole and outcrop data shows that fault boundaries and main structural elements can be correlated over a distance of 3.5–4.0 m. Within the Main Fault, the order of structural elements persists with a thin zone of scaly clay at the basis and a thick zone of scaly clay at the top with a separating zone of rhombohedral blocks in between, but their thicknesses varies considerably. Even though direct correlation of structural elements from an outcrop to a borehole located nearby seems to be simple, we note that the Main Fault features are highly non-planar. This is especially true for scaly clay, S–C bands, and microfolds. Patchy occurrence and lateral boudinage are quite common. A comparison of the Ga08E outcrop with the Ga08W outcrop (Fig. 6) shows the pronounced lateral variability that occurs along the Main Fault. Despite these restrictions, we

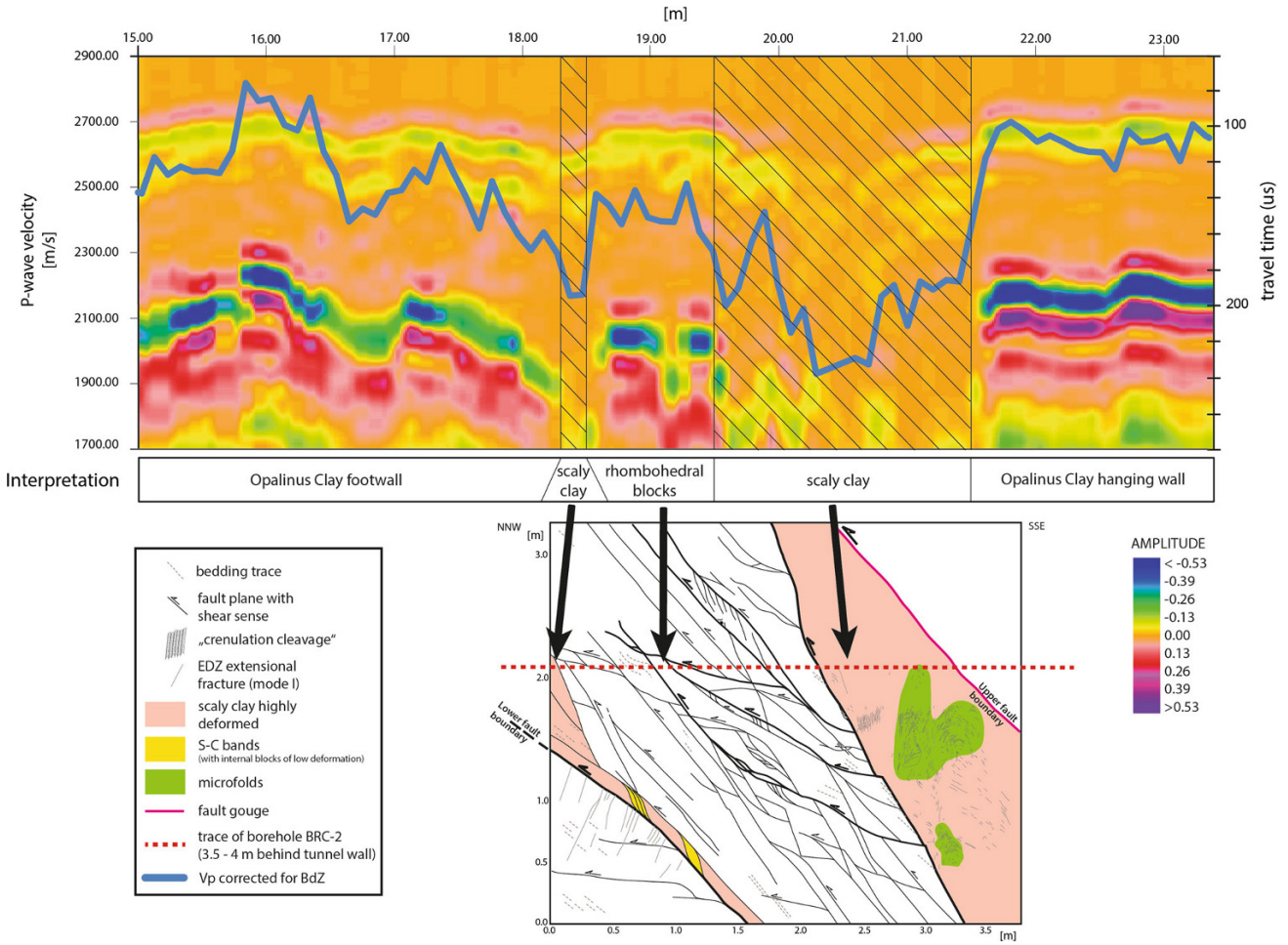

Fig. 7 Signal of BdZ-corrected Vp along trace of borehole BRC-2 correlated to structural elements of Main Fault Ga08E. The trace of BRC-2 is located ca. 3.5–4.0 m behind the tunnel wall. The BdZ-corrected Vp uses different emitter-receiver spacings, which represents a larger depth of penetration (Vp on *left vertical axis*). *Upper horizontal axis* marks borehole metre of BRC-2. In the background, a common offset gather (*COF*) is given, showing traveltime (μs) on the *right vertical axis* and relative *colour coded* amplitudes

can make some important findings: Vp, normalised amplitudes and elastodynamic parameters within the Main Fault are clearly reduced compared to undeformed Opalinus Clay. Also, upper and lower boundaries of the Main Fault can be recognised on the ultrasonic log. Thick zones of scaly clay (>0.2 m) exhibit lower Vp than the zone of rhombohedral blocks bound by slickensides. Consequently, at least for the Main Fault in Ga08, resolution of the ultrasonic measurements is sufficient for detection of internal boundaries within the Main Fault structure.

5 Interpretation and discussion

5.1 Structural elements of the Main Fault

The four outcrops of the Main Fault in the Mont Terri rock laboratory exhibit five macroscopic structural elements characterizing this Opalinus Clay fault zone. These are (1) scaly clay with (2) microfolds and (3) S–C bands, (4) gouge, and (5) rhombohedral blocks bound by slickensides. Slickensides are found in all the five structural elements and thus represent a major part of such fault zones. Slickensides are characterised by reduced porosity, aligned clay particles and patchy calcite as well as risers (Laurich 2015). Indicators of pressure solution are present at steps (e.g. truncated shell fragments).

Scaly clay is interpreted to be a product of continuous strain at geometrically locked positions, which occur within relays of two linking shears. Laurich (2015) showed that shear zone density increases with increasing strain. We observe no mineralogical change compared to the host rock. Scaly clay represents the highest strained parts of the Main Fault and occurs on all four outcrops especially at the upper and lower fault boundary. For the Main Fault, this geometrical occurrence of scaly clay at the fault boundaries implies that the fault core with highest strains is located at fault boundaries; whereas the central parts have

accommodated much less strain. Investigations performed on the Tournemire shale support this observation (Dick et al. 2016). Those authors reported that strain inferred from anisotropy of magnetic susceptibility measurements on a 1.5 m-thick fault zone indicated heterogeneous structural fabrics within the core of the fault zone. This core also exhibits subparallel, strongly deformed zones, such as gouge bands and scaly clay with isolated lenses of undeformed rock. A comparison of fault zone geometry between siliclastic sediments and siltstones yielded thinner deformation bands in the siltstones (Johansen and Fossen 2008). These authors furthermore reported that deformation bands, such as gouges or scaly clay, are unevenly distributed throughout the damage zone. At the outcrops in Ga98, scaly clay is present in the inner part of the fault. The abundance of scaly clay reduces gradually from the westernmost outcrop Ga08W (53%) to the outcrop Ga98E (20%). Table 1 clearly shows the correlation between thickness of the fault zone and areal coverage by scaly clay. The thinner the fault zone, the less abundant the scaly clay. This observation is somewhat contradictory for outcrops that are only 50 m apart and which should contain the same fault zone. Thus if similar strain rates or offsets for all four outcrops are assumed, the strain could, for instance, be more localized in the fault-gouge layers. Fault gouge might contribute differently to strain accommodation from one outcrop to the other. Alternatively, strain and total offset could decrease from western to eastern outcrops and partly be accommodated by rock matrix or by faults or fault zones parallel to the Main Fault. Different fault zone widths and area percentages of scaly clay suggest that (1) the major offset is accommodated by the thin gouge band leaving a highly variable macroscopic strain and (2) there are unrecognized, Main Fault parallel, fault zones in Ga98 that partly accommodate the offset. These deductions agree with observations in other galleries and boreholes where it is difficult to correlate the Main Fault over even short distances. At several locations in the rock lab (e.g. Gallery FE; Jaeggi et al. 2013) and in borehole BFE-E5 (Jaeggi et al. 2014), comparable fault zones with identical orientations and structural elements have been found, although it was impossible to correlate them laterally over larger distances. We postulate that fault zones in clay rocks exhibiting low stiffness and pronounced bedding anisotropy are inherently discontinuous and probably distribute offset along several parallel fault strands, each with a highly variable internal structure. At this larger scale, clay/shale fault zones probably have similar internal structures compared to those observed within the Mont Terri Main Fault, i.e. they consist of higher and lower-strained regions bounded by slickenside-dominated shear surfaces.

Scaly clay includes *S–C bands* and *microfolds*. Comparing the four outcrops shows that with reducing thickness of the fault zone, complexity of internal structure increases. In contrast, scaly clay in Ga08W exhibits only an anastomosing network of slickensides. We can detect no preferred orientation of the shears. Microfolds and S–C bands are present in the thinner exposures further east. Laurich (2015) showed that scaly clay internal microlithons are largely undeformed. Generally, scaly clay and its associated microfolds and shear bands occur at the upper and lower boundary of the fault zone. The Ga98W exposure presents an exception, where these structural elements are present within the central zone of rhombohedral blocks bound by slickensides. This exposure has three major internal faults subparallel to the Main Fault boundaries, and the internal structure is much more undulating, where it is difficult to determine the lower fault boundary. We postulate that the undulating behaviour together with the internal major faults parallel to the boundaries led to geometric locking with subsequent strain concentrations at internal locations. This enabled the formation of scaly clay and associated deformation structures.

Fault gouge is associated with the scaly clay and is commonly located at the upper boundary of the Main Fault (hanging wall) with highest strain occurring in very narrow bands. Microscopic investigations by Laurich (2015) have shown that the dark colour of the gouge results from grain size reduction, reduced porosity, and calcite depletion. Veins inside the gouge are rare, but occur frequently along gouge boundaries. This could indicate that gouge acts as a low permeability zone (permeability barrier) during formation of fault zones. Furthermore, Laurich (2015) demonstrated that these veins are frequently healed and occasionally strained, suggesting a frictional-viscous deformation mechanism assisted by pressure solution. Macroscopically, only fault gouges at the upper boundary of the Main Fault are mappable. Microscopically, gouge is also found in scaly clay samples far from fault zone boundaries (Laurich 2015).

In their work on the Barbados prism, Housen et al. (1996) proposed that most strain in the décollement has been accumulated by the volumetrically minor component of shear zones. We can confirm this statement at Mont Terri on a much smaller scale, where we observe the occurrence of a low area percentage of highly deformed scaly clay and gouge compared to zones of undeformed host rock within the Main Fault. At Mont Terri, the internal zones of the Main Fault are characterized by mostly undeformed *rhombohedral blocks* bound by µm-thick slickensides. A comparison of the different outcrops clearly shows reduction of block size from the largest in Ga08W towards those in Ga98. Furthermore, the area percentage of the zone with isolated slickensides clearly increases with decreasing thickness of the fault zone: 47% for Ga08W vs. 80% for Ga98E. The abundance of scaly clay in turn

decreases. This behaviour is not straightforward since the zone with blocks bound by slickensides accommodates much less strain than scaly clay. However, the reduction in block size with decreasing thickness of the fault zone can be explained by strain accommodated across a much thinner zone. We note that the mapping detail possible at Ga08W was less than for the other exposures, which could at least partly explain the larger block size of the internal zone.

Calcite veins, μm-shear zones, and gouge show decreased porosity and are thought to act as local seals during evolution of the fault zone (Laurich et al. 2014; Laurich 2015). In a rock with very low-permeability where on the short-term pore water cannot escape, further shearing leads to localized increase of the pore water pressure. An increase in pore-water pressure shifts the Mohr's stress circle to the left or towards failure at smaller normal stresses, favouring generation of new shears (Gudmundsson 2001). This localized pressure build-up can hypothetically cause development of a dense shear zone network, as for scaly clay (Vannucchi et al. 2003). Thus in parts of the Main Fault, these seals might have led to intra-fault pore pressure increase that finally caused formation of the complex anastomosing shear zone network of scaly clay. Laurich et al. (2016) propose a model to explain the progressive formation of a self-similar network of anastomosing thin shear zones during continuous deformation. According to these authors, evolution of the initial segments of the Main Fault can be explained by localized deformation that has interacted with slip along rotated bedding foliation. Due to fault geometry, geometric locking leads to stress concentrations, initiating new shear zones. Laurich et al. (2016) propose that these initial shear zone networks develop into fault segments, which coalesce during further fault movement. Such an evolution leads inevitably to the assumed heterogeneous strain distribution across the Main Fault. Based on our geometrical observations on the Main Fault with varying fault zone thickness and strain localization in structural elements such as gouge and scaly clay, we furthermore propose that geometric locking leads to microcracking and dilatancy, which provoked intermittent local pore pressure drops. During such pressure drops, lateral stress transfer across the undeformed rock matrix to domains out of the mapped Main Fault zone could have occurred. There again similar fault geometries could have developed at parallel fault strands initiated by bedding-parallel slip combined with rotation of bedding foliation.

P-wave velocity (Vp) of borehole BRC-2 can clearly be correlated to the internal structure of the Main Fault in Ga08. From 18.3 to 21.5 m Vp is consistently reduced with respect to undeformed Opalinus Clay (Fig. 7). The scaly clay at the lower fault boundary (footwall) leads to a pronounced decrease of Vp and a change in the COF trace plot. Geophysical investigations can therefore resolve scaly clay of 20 cm thickness in borehole BRC-2, which probably is close to the theoretical upper limit of resolution. Rhombohedral blocks bound by slickensides are damping amplitude and decreasing seismic velocity when compared to the undeformed host rock. However, Vp is still higher than in scaly clay. It is not surprising that the thick zone of scaly clay with highest density of slickensides in various orientations exhibits the lowest seismic velocities. The anastomosing, uncemented structure attenuates ultrasonic waves, despite decreased porosity. In addition to mineralogy and cementation, fabric has a major influence on ultrasonic signals (Schuster et al. 2017). We postulate that thicker zones of scaly clay (>0.2 m) and rhombohedral blocks bound by slickensides can be detected and distinguished with ultrasonic measurement. Thus, under ideal circumstances these geophysical tools can resolve the internal structure of the Main Fault.

5.2 Generic block model of the Main Fault at Mont Terri

Macroscopic comparison of the four exposures combined with microscopic investigations by Laurich (2015) enables us to derive a generic model for the Main Fault of the Mont Terri rock laboratory. The block model shows the most important features of the Main Fault (Fig. 8). It is representative for the Main Fault in Ga08 and Ga98E. Ga98W is more complex with a slightly different spatial distribution of structural elements. Upper and lower fault boundaries are bound by structural elements, which probably accommodated most of the strain. The gouge at the top of the Main Fault is continuous. Microscopic investigations of different exposures of gouge have shown sharp boundaries with the host rock emphasising host rock abrasion and calcite dissolution in a μm-thin, gouge-bounding Y-shear. Two types of gouge have been found, differing in P-foliation angle. The type with P-foliation subparallel to the shear zone dip is inferred to represent a mature gouge, while the type with P-foliation oblique to the shear zone dip is interpreted as young gouge. In agreement with this interpretation, the latter type has more unreworked host rock clasts than the first type. Scaly clay is always adjacent to gouge, occasionally in aggregates as thick as 1 m. It is appealing to hypothesise that gouge has formed by ongoing deformation of the scaly clay. Apart from rather small regions of microfolds and S–C bands, anastomosing networks of shear zones dominate the internal structure of scaly clay. For all these structural elements, slickensides are the elementary building blocks. Except for the thick upper zone of scaly clay in Ga08, there is a much thinner

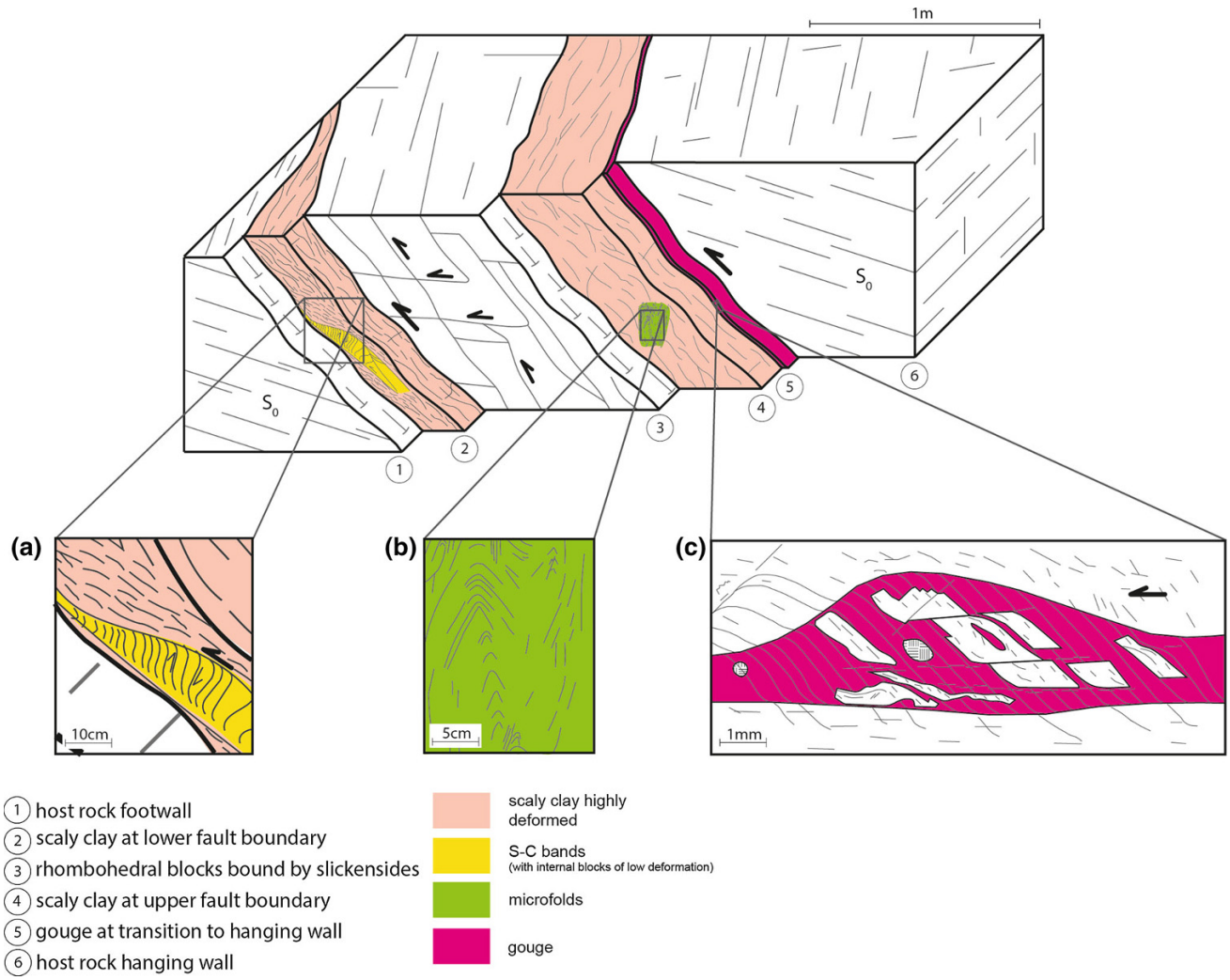

Fig. 8 Generic block model of the Main Fault in the Opalinus Clay of the Mont Terri rock laboratory showing the structural elements and their distribution. Close-ups: **a** S–C bands with internal sigmoidal structure, **b** microfolds within scaly clay, **c** gouge as observed at upper boundary of Main Fault (adapted after Laurich 2015)

(<20 cm) zone of scaly clay at the lower boundary of the Main Fault. At the base (footwall) of the Main Fault, S–C bands are common and contain internal, largely undeformed microlithons. Again, except for the exposure in Ga08W this lower band of scaly clay seems to be continuous. The colours of the model (Fig. 8) highlight the amount of strain accommodated, which is highest for the dark red (gouge), intermediate to high for light red (scaly clay and associated microfolds and S–C bands), and lowest for the uncoloured parts, such as rhombohedral blocks bound by slickensides and the undeformed wall rock.

6 Conclusions

We can identify five structural elements at outcrop scale and have established a generic block model that encompasses the observed macroscopic features of a fault zone within the Opalinus Clay. Scaly clay is observed as isolated aggregates within the Main Fault and at its upper (hanging wall) and lower (footwall) boundaries. Scaly clay includes microfolds and S–C bands. A continuous gouge band of up to 2 cm thickness runs along the upper boundary of the Main Fault. The non-scaly, inner part of the Main Fault consists of rhombohedral blocks bound by slickensides.

We found identical orientations and structural elements throughout the rock laboratory. However, lateral correlation of structural elements over larger distances is impossible. Comparison of relative area percentages of structural elements among the four exposures analysed shows that with decreasing fault zone thickness, the area percentage of the zone with isolated slickensides increases, whilst the abundance of scaly clay decreases. Reduction of block size with decreasing thickness of the fault zone can be explained by the amount of strain accommodated across a much thinner zone.

We postulate that fault zones in clay rocks with low stiffness and pronounced bedding anisotropy are inherently discontinuous and probably distribute offset along several parallel fault strands, each with a highly variable internal structure. A model for the evolution of such fault zones, which is consistent with our observations on fault geometry and distribution of structural elements, is proposed by Laurich et al. (2016).

Correlation of Vp with structural elements of the Ga08E outcrop shows a clear relationship to the internal structure of the Main Fault. Given the strong correlation between outcrop and geophysical borehole data, we can use ultrasonic geophysical measurements to deduce the internal structure of the Mont Terri Main Fault to a high degree of fidelity.

Acknowledgements The authors would like to thank the Mont Terri Project Partners swisstopo and Chevron for their financial contribution to the PS (Petrofabric and Strain) experiment. Both reviewers Marco Herwegh from University of Bern and Reto Thöny from AF Consult provided useful comments and helped to improve the manuscript. We thank Fabian Jäggi, Solothurn, for creating and improving the figures of this work.

References

Baur, S. (2014). *Geological, Petrophysical and Geochemical Investigations of the Opalinus Clay Formation of the Underground Rock Laboratory Mont Terri, Switzerland. Master thesis*, Albert-Ludwigs-University of Freiburg, Freiburg in Breisgau, Germany.

Blaesi, H. R., Moeri, A., & Bossart, P. (1996). *Results of the Phase 1 drilling campaign. Mont Terri Technical Report*, TR96-01. Federal Office of Topography (swisstopo), Wabern, Switzerland. http://www.mont-terri.ch.

Blenkinsop, T. G. (2000). *Deformation microstructures and mechanisms in minerals and rocks* (p. 150). Dordrecht: Kluwer Academic Publishers.

Bossart, P., Bernier, F., Birkholzer, J., Bruggeman, C., Connolli, P., Dewonck, S., et al. (2017). Mont Terri rock laboratory, 20 years: Introduction, site characteristics and overview of experiments. *Swiss Journal of Geosciences, 110*. doi:10.1007/s00015-016-0236-1.

Bossart, P., & Thury, M. (2008). *Mont Terri Rock Laboratory. Project, programme 1996 to 2007 and results*. *Reports of the Swiss Geological Survey*, *3*. Federal Office of Topography (swisstopo), Wabern, Switzerland. http://www.mont-terri.ch.

Chester, F. M., Rowe, C., Ujiie, K., Kirkpatrick, J., Regalla, C., Remitti, F., et al. (2013). Structure and composition of the plateboundary slip zone for the 2011 Tohoku-Oki earthquake. *Science, 342,* 1208–1211.

Clauer, N., Techer, I., Nussbaum, C., & Laurich, B. (2017). Geochemical signatures of paleofluids in microstructures from Main Fault of the Opalinus Clay, Mont Terri rock laboratory (Switzerland). *Swiss Journal of Geosciences, 110* (this issue).

Dick, P., Wittebroodt, C., Courbet, C., Sammaljärvi, J., Estève, I., Matray, J.-M., et al. (2016). The internal architecture and permeability structures of faults in shale formations. *The Clay Minerals Society Workshop Lectures Series, 21*(17), 227–242.

Dielforder, A., Vollstaedt, H., Vennemann, T., Berger, A., & Herwegh, M. (2015). Linking megathrust earthquakes to brittle deformation in a fossil accretionary complex. *Nature Communications, 6,* 7504.

Doblas, M., Mahecha, V., & Hoyos, M. (1997). Slickenside and fault surface kinematic indicators on active normal faults of the Alpine Betic cordilleras, Granada, southern Spain. *Journal of Structural Geology, 19,* 159–170.

Gratier, J.-P., Renard, F., & Vial, B. (2014). Postseismic pressure solution creep: Evidence and time-dependent change from dynamic indenting experiments. *Journal of Geophysical Research Solid Earth, 119,* 2764–2779.

Gschwind, S. (2013). *The Relationship between Failure Behavior and Sedimentary Subfacies Types in the Sandy Facies of Opalinus Clay. Master thesis*, Swiss Federal Institute of Technology in Zurich (ETH Zurich), Zurich, Switzerland.

Gudmundsson, A. (2001). Fluid overpressure and flow in fault zones: Field measurements and models. *Tectonophysics, 336,* 183–197.

Haines, S. H., Kaproth, B., Marone, C., Saffer, D., & van der Pluijm, B. (2013). Shear zones in clay-rich fault gouge: A laboratory study of fabric development and evolution. *Journal of Structural Geology, 51,* 206–225.

Hostettler, B., Reisdorf, A. G., Jaeggi, D., Deplazes, G., Blaesi, H. R., Morard, A., et al. (2017). Litho- and biostratigraphy of the Opalinus Clay and bounding formations in the Mont Terri rock laboratory (Switzerland). *Swiss Journal of Geosciences, 110*. doi:10.1007/s00015-016-0250-3

Houben, M. E., Desbois, G., & Urai, J. L. (2013). Pore morphology and distribution in the Shaly facies of Opalinus Clay (Mont Terri, Switzerland): Insights from representative 2D BIB–SEM investigations on mm to nm scale. *Applied Clay Science, 71,* 82–97.

Housen, B. A., Tobin, H. J., Labaume, P., Leitch, E. C., & Maltman, A. J. (1996). Strain decoupling across the decollement of the Barbados accretionary prism. *Geology, 24,* 127–130.

Ismat, Z. (2013). Block-supported cataclastic flow within the upper crust. *Journal of Structural Geology, 56,* 118–128.

Jaeggi, D., Lisjak, A., Gisiger, J., & Becker, J. (2013). FE-C experiment: Engineering part of full-scale emplacement experiment. Geological and structural mapping of the FE-tunnel including a photogrammetric method. *Mont Terri Technical Note*, TN2012-82. Federal Office of Topography (swisstopo), Wabern, Switzerland. http://www.mont-terri.ch.

Jaeggi, D., Wymann, L., Burrus, F., Becker, J., & Bossart, P. (2014). FE-E (EDZ-characterization in the vicinity of the FE-gallery) experiment. Synthesis of the excavation damaged zone (EDZ). *Mont Terri Technical Note*, TN2014-33. Federal Office of Topography (swisstopo), Wabern, Switzerland. http://www.mont-terri.ch.

Johansen, T. E. S., & Fossen, H. (2008). Internal geometry of fault damage zones in interbedded siliciclastic sediments. In C. A. J. Wibberley, W. Kurz, J. Imber, R. E. Holdsworth, & C. Collettini (Eds.), *The internal structure of fault zones: Implications for mechanical and fluid-flow properties* (pp. 35–56). London: The Geological Society of London.

Klinkenberg, M., Kaufhold, S., Dohrmann, R., & Siegesmund, S. (2009). Influence of carbonate microfabrics on the failure strength of claystones. *Engineering Geology, 107,* 42–54.

Koehn, D., & Passchier, C. W. (2000). Shear sense indicators in striped bedding-veins. *Journal of Structural Geology, 22,* 1141–1151.

Labaume, P., Maltman, A. J., Bolton, A., Tessier, D., Ogawa, Y., & Takizawas, S. (1997). Scaly fabrics in sheared clays from the decollement zone of the Barbados accretionary prism. In T. R. Shipley, Y. Ogawa, P. Blum, J. M. Bahr (Eds.), *Proceedings of the ocean drilling program* (pp. 59–77). USA: Texas A&M University.

Laurich, B. (2015). *Evolution of microstructure and porosity in faulted Opalinus Clay. PhD thesis*, RWTH Aachen University, Aachen, Germany.

Laurich, B., Urai, J. L., Desbois, G., Vollmer, C., & Nussbaum, C. (2014). Microstructural evolution of an incipient fault zone in Opalinus Clay: Insights from optical and electron microscopic study of iron-beam polished samples from the Main Fault in the Mont Terri underground research laboratory. *Journal of Structural Geology, 67,* 107–128.

Laurich, B., Urai, J. L., & Nussbaum, C. (2016). Microstructures and deformation mechanisms in Opalinus Clay: Insights from scaly clay from the Main Fault in the Mont Terri Rock Laboratory (CH). *Journal Solid Earth*. doi:10.5194/se-2016-94.

Marschall, P., Croisé, J., Schlickenrieder, L., Boisson, J.-Y., Vogel, P., & Yamamoto, S. (2004). Synthesis of hydrogeological investigations at the Mont Terri Site (phases 1 to 5). In P. Heitzmann (Ed.), *Mont Terri Project—Hydrogeological synthesis—Osmotic flow*. Bern: Reports of the Federal Office for Water and Geology, Geology Series, 6.

Marschall, P., Gimmi, T., & Horseman, S. (2005). Characterisation of gas transport properties of the Opalinus Clay. *Oil & Gas Science and Technology, 60,* 121–139.

Nussbaum, C., Bossart, P., Amann, F., & Aubourg, C. (2011). Analysis of tectonic structures and excavation induced fractures in the Opalinus Clay, Mont Terri underground rock laboratory (Switzerland). *Swiss Journal of Geosciences, 104,* 187–210.

Nussbaum, C., Bossart, P., Zingg, A., Inderbitzin, L., & Steiger, H. (2001). *Géométrie et cinématique d'une zone de chevauchement („Main Fault") recoupant les Argiles à Opalinus dans le laboratoire souterrain du Mont Terri. Mont Terri Technical Report*, TR2001-04. Federal Office of Topography (swisstopo), Wabern, Switzerland. http://www.mont-terri.ch.

Passchier, C. W., & Trouw, R. A. J. (1996). *Microtectonics*. Berlin: Springer.

Schuster, K. (2012). Detection of borehole disturbed zones and small scale rock heterogeneities with geophysical methods. In X. Li, L. Jing, & P. Blaser (Eds.), *Proceedings of the EC-TIMODAZ-THERESA International Conference, Impact of thermo-hydro-mechanical chemical (THMC) processes on the safety of underground radioactive waste repositories, Luxembourg, 29 Sep.–1 Oct. 2009* (pp. 135–145). Publications Office, 2012.

Schuster, K., Amann, F., Yong, S., Connolly, P., & Bossart, P. (2017). High-resolution mini-seismic methods applied in the Mont Terri rock laboratory (Switzerland). *Swiss Journal of Geosciences, 110*. doi:10.1007/s00015-016-0241-4.

Thoeny, R. (2014). *Geomechanical analysis of excavation-induced rock mass behavior of faulted Opalinus Clay at the Mont Terri Underground Rock Laboratory (Switzerland). PhD thesis,* Swiss Federal Institute of Technology in Zurich (ETH Zurich), Zurich, Switzerland.

Vannucchi, P., Maltman, A., Bettelli, G., & Clennell, B. (2003). On the nature of scaly fabric and scaly clay. *Journal of Structural Geology, 25,* 673–688.

Yong, S., Kaiser, P. K., & Loew, S. (2010). Influence of the tectonic shears on tunnel-induced fracturing. *International Journal of Rock Mechanics and Mining Sciences, 47,* 894–907.